Charge Transfer from Metallic Single-Walled Carbon Nanotube Sensor Arrays

Chang Young Lee,[†] Seunghyun Baik,[‡] Jianqi Zhang,[†] Richard I. Masel,[†] and Michael S. Strano*,[†]

Department of Chemical and Biomolecular Engineering, University of Illinois at Urbana-Champaign, Urbana, Illinois 61801, and School of Mechanical Engineering, Sungkyunkwan University, Suwon 440-746, Korea

Received: November 7, 2005; In Final Form: March 22, 2006

This paper explores the possibility of using arrays of metallic carbon nanotubes as sensors. Unlike their semiconducting counterparts, single-walled carbon nanotube arrays or networks that are dominated by metallic conduction pathways have not been investigated for their environmental sensitivity. In this work, we demonstrate transduction of molecular adsorption via charge transfer through predominantly metallic single-walled carbon nanotubes. Raman spectroscopy and electric field dependent transport confirm that signal transduction takes place through primarily large diameter metallic nanotubes. This unique signal transduction mechanism might have implications for novel sensors. The scaling of the signal with array impedance is well described using an irreversible binding model developed previously. The arrays have several advantages including a simple, two-electrode fabrication, rapid regeneration, and a responsivity that scales predictably and linearly with the number of adsorption sites. An array-assisted hydrolysis of reactive analytes is found to regenerate the nanotube surface from hydrolyzable species which include important organophosphate nerve agents.

Introduction

All atoms of single-walled carbon nanotubes (SWNTs) reside at the surface making them promising and widely explored sensor elements.[1−6] Early prototypes have been based on field effect transistors (FETs)[1,7−9] where drain currents can be modulated by the adsorption of electron-withdrawing/donating molecules that change the charge carrier density.

Several analytes have been detected at sub-parts per million levels, such as nitrous oxide,[1,10,11] ammonia,[1,11−13] and dimethyl methylphosphonate (DMMP).[12,14] A longstanding problem with nanotube gas and vapor sensors is that molecular adsorption is largely irreversible, requiring an active means of regeneration including UV irradiation,[1,15] heat treatment,[11] or gate bias.[12] We have previously published a detailed analysis of irreversible binding to nanotube sensors for several systems that have appeared in the literature.[16] Even a novel gas sensor based on carbon nanotube capacitance[14] exhibits irreversible changes in its impedance upon molecular binding.

A number of ways for improving sensitivity and selectivity, including polymer coatings,[1,9,12,13] doping,[3] or loading metal nanoparticles,[15] have been studied as well. However, in these studies, it has been unclear as to what quantity should be examined to optimize the sensor response. Typically, the normalized conductance change ($\Delta G/G_0$) has been examined but with little or no link to the chemical or physical properties of the analyte or carbon nanotube array. Density functional theoretical calculations[3,17] on single nanotubes have been performed suggesting changes in the nanotube density of states by analyte adsorption. However, the connection to actual sensor responses is not known.

SWNTs are either metallic or semiconducting depending upon their chirality.[18,19] In particular, utilizing semiconducting carbon nanotubes whose conductance can be easily turned on and off by chemical doping has become the primary transduction mechanism.[8,11,20] The Schottky barrier FET[21] model implies that the origin of the semiconducting nanotube sensor response is derived in part from the modulation of the Schottky barrier at the metal electrodes/nanotube contact. The role of this contact has been experimentally studied using contact-passivated devices.[20] Semiconducting nanotubes are thought to be more sensitive than metallic because the total range of available signal transduction for the latter spans the on/off ratio of several orders of magnitude. Accordingly, the explicit function of metallic SWNTs in sensor applications, and particularly in SWNT networks, has received little attention.

In this work, we examine the environmental response of SWNT arrays in response to molecular adsorption where the percolation of metallic nanotubes dominates the transport behavior. Both thionyl chloride ($SOCl_2$) and DMMP, which are a nerve agent precursor and simulant, respectively, are investigated. The arrays are fabricated using ac (alternating current) dielectrophoresis.[22,23] Experimentally, the current through the nanotube network is shown to be directly proportional to the number of nanotubes on the array. Vertical shifts in this linear relationship are observed for different configurations and analytes ($SOCl_2$ and DMMP). The results are explained using an analysis previously developed.[16] To verify the signal transduction mechanism, Raman spectroscopy and electrical transport measurements before and after analyte exposure are performed. We conclude from these measurements that the charge transfer between $SOCl_2$ and carbon nanotubes occurs uniquely through a metallic pathway. Signal increase by $SOCl_2$ adsorption is attributed to the high density of states at low Fermi level along with enhanced electron tunneling at the nanotube/electrode contact. The surface can be regenerated by an array-assisted hydrolysis. Our results imply the potential application of metallic nanotube arrays as gas sensing elements.

* To whom correspondence should be addressed. E-mail: strano@uiuc.edu.

[†] University of Illinois at Urbana-Champaign.

[‡] Sungkyunkwan University.

10.1021/jp056425v CCC: $33.50
Published on Web 05/20/2006

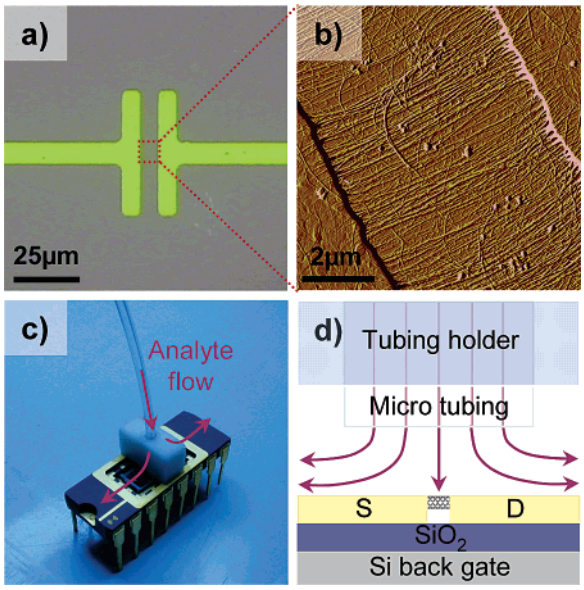

Figure 1. (a) Optical image of 6 μm gap Au electrodes. (b) AFM image of HiPco nanotubes deposited on the gap by ac dielectrophoresis. (c) Setup for analyte delivery: diced substrate is mounted and wirebonded to a dual in-line package (DIP). Analyte is delivered perpendicularly to the substrate via the microtubing and is free to leave the setup. (d) Schematic of analyte delivery onto the SWNT array. The area ratio of the tubing to the gap determines the efficiency of analyte delivery.

Experimental Section

Silicon substrates (Montco Silicon Technologies) with 150 nm thermal oxide were metallized with 5 nm Ti and 300 nm Au, where electrodes with 3 or 6 μm gaps (Figure 1a) were patterned by photolithography. Alternating current dielectophoresis was performed to form a nanotube array between the gaps (Figure 1b) as follows: 3 μL of HiPco carbon nanotube (Rice University) suspension (16.4 mg/L in 1% sodium dodecyl sulfate (SDS)-H_2O) prepared as described previously[24] was dropped on the gap. An ac voltage of 12 V_{pp} (3 μm gap) or 15 V_{pp} (6 μm gap) at 10 MHz was applied. The droplet was blown off, and the power was turned off. Although the control of SWNT coverage was attempted by varying deposition time (3−10 min), the array impedances ranged from 1.3 to 494 μS even at the same deposition time (3 min). The substrate was rinsed with deionized water to remove residual SDS. DNA $(d(GT)_{15})$[25]-suspended HiPco (6.64 mg/L in H_2O) nanotubes were prepared and deposited in a similar way. The configuration allowed testing of the array field effect.[1,7−9] Variations in electric field and deposition time result in different numbers of nanotubes in the channel. All nanotube suspensions were dialyzed prior to dielectrophoresis to minimize excess ions and surfactants in the solution.

PFA (perfluoroalkoxy) micromedical tubing (ID = 0.457 mm, Scientific Commodities, Inc.) was aligned and glued such that it was suspended above the gap for analyte delivery (Figure 1c). Delivered analyte molecules are free to leave the setup to the open air. This simple and disposable setup prevents contamination from highly corrosive thionyl chloride molecules. The analyte flow is perpendicular to the nanotube surface (Figure 1d). Only 0.2% of the total analyte is estimated to flow directly onto the gap from hydrodynamic analysis; it is noted that smaller diameter tubing or large gap electrodes could improve the efficiency of analyte delivery.

Desired $SOCl_2$ concentrations were obtained by vaporizing 2.0 M $SOCl_2$ (solution in dichloromethane, Sigma Aldrich) diluted in dichloromethane (Sigma Aldrich) in dry flasks filled with ultrahigh-purity nitrogen. DMMP analyte was prepared by diluting saturated vapor with the air.

Current−voltage measurements were performed using a semiconductor parameter analyzer (HP4155 and E5272A, Agilent). While monitoring the current at a source-drain bias voltage of 1 mV, a pulse of 3 mL of analyte vapor was injected for 10 s (0.3 mL/s) through the microtubing. Raman spectra at the excitation laser wavelengths of 632.8 nm (1 mW at sample) and 785 nm (37.5 mW at sample) were also obtained before and after exposure to $SOCl_2$, with a Kaiser RamanRXN1 analyzer.

Results and Discussion

Figure 2a shows a typical response to 3 mL of 100 ppm $SOCl_2$ pulsed for 10 s at a source-drain bias voltage of 1 mV. There is a rapid increase in the current upon analyte injection. The signal increases for approximately 10 s upon injection of the analyte. Approximately 25% of the signal was restored after 50 s, suggesting desorption of analyte molecules. This type of response is identical to that of an array reported previously.[12] From an analysis of multiple devices, it is observed that the signal does not restore after more than 4 h. The kinetics of analyte adsorption for these systems is independent of analyte flow rate unless the system is diffusion-limited. The response to the dichloromethane solvent is negligible.[26] Multiple injections give a stepwise increase in the current as expected for an irreversibly binding analyte.[27] These results suggest that the $SOCl_2$ binding event is at least partially irreversible as observed with several other analytes on SWNT sensors.[16]

To link the conductance change to array and analyte properties, each device was tested using an identical pulse of 100 ppm $SOCl_2$ or DMMP. The initial conductance before the analyte injection (G_o) and the amount of conductance change upon exposure to the analyte (ΔG) were both measured. Figure 2b shows the relationship between G_o and ΔG from three surfactant/analyte combinations for 34 devices. Three systems were investigated: (1) the $SOCl_2$ response from SDS-suspended nanotubes (3 or 6 μm gap),[28] (2) the $SOCl_2$ response from DNA-suspended nanotubes (6 μm gap), and (3) the DMMP response from SDS-suspended nanotubes (6 μm gap). Only system 3 showed negative responses. All responses fall on a straight line with a slope of unity but with different intercepts on a log−log plot.[29] This unity slope corresponds to a constant $\Delta G/G_o$ value at a fixed analyte concentration. The intercept values on the ΔG axis are −0.2105, −0.8291, and −1.479 for systems 1, 2, and 3, respectively.

Atomic force microscopy (AFM) images were taken from three devices with representative G_o values (Figure 2c). It is noted that the initial conductance becomes higher as the number of nanotubes increases. Therefore, we interpret the results in Figure 2b in terms of the number of adsorption sites as suggested previously.[16] We assume, for simple analysis, the response in Figure 2a is totally irreversible. The total number of sites on nanotubes available for molecular adsorption is $T\theta$. A gas-phase analyte molecule (A) with concentration C_a adsorbs on the nanotube surface filling $A\theta$ sites and leaving θ sites unoccupied. For irreversible adsorption

$$A(g) + \theta(sur) \xrightarrow{k} A\theta(sur) \qquad (1)$$

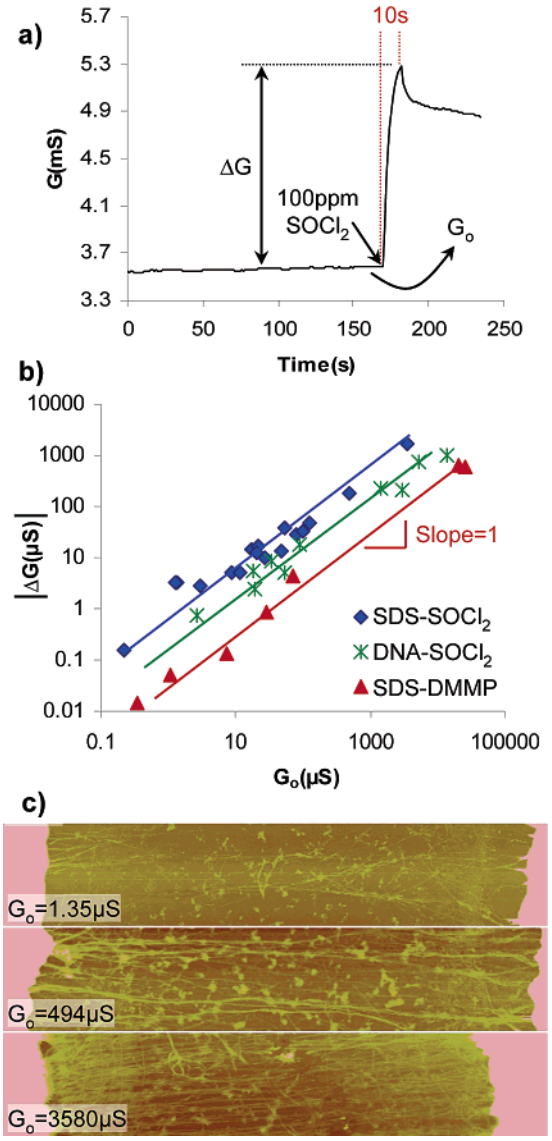

Figure 2. (a) Typical conductance change due to 3 mL of 100 ppm $SOCl_2$ pulsed for 10 s. $SOCl_2$ adsorption is partially irreversible. G_o and ΔG are related to the number of carbon nanotubes crossing the gap and the amount of $SOCl_2$ molecules adsorbed on the nanotubes, respectively. (b) ΔG from 34 devices plotted vs G_o. $SOCl_2$ responses from SDS-SWNT fall on a straight line with slope 1 for both the 3 and 6 μm gaps. $SOCl_2$ responses from DNA−SWNT and DMMP responses from SDS−SWNT show the same linear relationship with different intercepts. The unity slope corresponds to a constant normalized conductance ($\Delta G/G_o$) at a fixed concentration. The intercept determines the selectivity and sensitivity for a particular analyte. (c) AFM images (8 μm × 1.5 μm) from devices with different initial conductance values. The G_o value increases with the number of nanotubes.

Here, k is the adsorption rate constant, with g and sur denoting the gas-phase and surface bound species, respectively. The number of sites on nanotubes remains constant.

$$\theta(\mathrm{sur}) + \mathrm{A}\theta(\mathrm{sur}) = \mathrm{T}\theta(\mathrm{sur}) \quad (2)$$

$\mathrm{A}\theta$ can be derived from eqs 1 and 2 for an initially clean array.

$$\frac{d\mathrm{A}\theta}{dt} = k\theta C_a = k(\mathrm{T}\theta - \mathrm{A}\theta)C_a \quad (3)$$

$$\mathrm{A}\theta = (\mathrm{T}\theta)(1 - \exp[-kC_a t]) \quad (4)$$

TABLE 1: Adsorption Rate Constant (k) and Maximum Conductance Change ($(\Delta G/G_o)_{Max}$) for the Three Systems Tested[a]

surfactant	analyte	C_a (ppm)	intercept	k ($ppt^{-1}\ s^{-1}$)	$(\Delta G/G_o)_{max}$
SDS	$SOCl_2$	100 50 10	−0.2105 −0.5486 −0.8838	2.69×10^{-9}	0.533
DNA	$SOCl_2$	100 50	−0.8291 −1.040	9.41×10^{-10}	0.243
SDS	DMMP	100 50	−1.479 −1.556	3.29×10^{-9}	0.0345

[a] Responses at two different concentrations are sufficient to calculate both parameters from intercept values in the $\log(\Delta G)$ vs $\log(G_o)$ graph. The sensitivities are different although the rates of analyte adsorption are similar in all systems.

G_o is proportional to the number of nanotubes crossing the gap and, thus, to the total number of adsorption sites ($\mathrm{T}\theta$) available. ΔG is proportional to the number of analyte molecules adsorbed on nanotubes crossing the gap.

$$\mathrm{T}\theta = \alpha G_o$$

and

$$\mathrm{A}\theta = \beta \Delta G \quad (5)$$

Here, α and β are proportionality constants. Therefore, assuming the same sticking coefficient[30] for each nanotube array, a device with more nanotubes is expected to show a higher current increase at a fixed concentration. The ratio α/β can be found in terms of maximum conductance change ($(\Delta G/G_o)_{max}$) when all the sites are occupied by analyte molecules ($\mathrm{A}\theta = \mathrm{T}\theta$).

$$\frac{\alpha}{\beta} = \left(\frac{\Delta G}{G_o}\right)_{max} \quad (6)$$

At constant concentration ($C_a = 100$ ppm) and time ($t = 10$ s), eq 4 can be rewritten as

$$\log \Delta G = \log\{(\Delta G/G_o)_{max}[1 - \exp(-kC_a t)]\} + \log G_o \quad (7)$$

Hence, when plotted on a log−log scale, ΔG and G_o should have a unity slope as suggested experimentally in Figure 2b. The intercept values are related to the maximum available signal change and provide the sensitivity and selectivity of a device for a specific analyte. This suggests a simple procedure of sensor optimization: (1) prepare sensors with different configurations, (2) test one of each configuration at the same concentration, and (3) use a configuration with the highest $((\Delta G/G_o)_{max}$.

We hypothesize that DNA wrapping around nanotubes, unlike SDS molecules,[31] is relatively stable in a water rinse. Hence, in Figure 2b, the smaller intercept value for DNA−SWNT could be explained by a reduction in surface area by residual DNA molecules. The low intercept value in the case of DMMP indicates a uniformly greater response to $SOCl_2$.

Plotting $\log(\Delta G)$ vs $\log(G_o)$ at two different analyte concentrations yields two important parameters of a nanotube array, the maximum signal ($(\Delta G/G_o)_{max}$) and analyte adsorption rate constant (k). A total of 71 nanotube devices including the 34 plotted in Figure 2b were tested to confirm this linear relationship and obtain k and $(\Delta G/G_o)_{max}$. The results are summarized in Table 1.[32] The k values are of the order 10^{-9}/ppt (parts per trillion)·s for all three types suggesting similar rates of analyte adsorption for each system. The systems vary in $(\Delta G/G_o)_{max}$ values. The values for k and $(\Delta G/G_o)_{max}$ are related, respectively, to the rate and magnitude of the signal transduction.

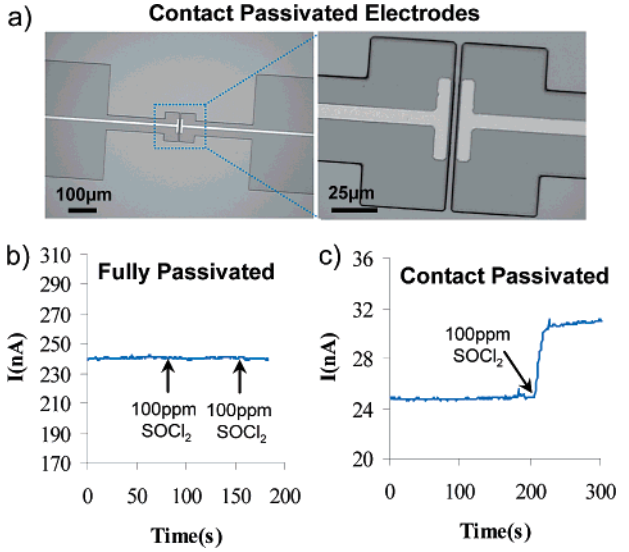

Figure 3. Response from a contact-passivated SWNT device. (a) Both electrodes and electrode/nanotube contacts are passivated with SU8-2 photoresist exposing only nanotubes to the analyte. (b) The passivated region is completely isolated from the analyte as shown by a zero response from the fully passivated device. (c) The response from the contact-passivated array matches the trend line in Figure 2b. These results confirm the negligible role of metal/nanotube contact in the signal transduction.

Compared to a previously analyzed system ($k \sim 10^{-6}$/ppt·s, $(\Delta G/G_o)_{max} \sim 0.43$),[16] k is smaller by 3 orders of magnitude, but with a slightly higher $(\Delta G/G_o)_{max}$ for our SDS−$SOCl_2$ system.

As described in the work on oxygen sensors by Heinze et al.,[21] one of the important issues in unveiling the origin of the nanotube sensor response is the work function modulation by the adsorbate and thus the modulation of the Schottky barrier. In this work, the role of the electrode/nanotube contact in $SOCl_2$ response was investigated. Negative photoresist (SU8-2, MicroChem) was used for patterning passivation layers (~1.5 μm thick) over the electrodes (Figure 3a). No response was observed when both electrodes and nanotubes were covered and the system was exposed to the analyte (Figure 3b). Hence, the passivation scheme was effective. Contact-passivated arrays, where only nanotubes were exposed, still exhibited a 24% increase in conductance (Figure 3c). Considering that approximately 47% of the gap is passivated, this is 72% of the expected signal from the trend line in Figure 2b. The 28% decrease in sensitivity could be from the lithographic procedure or a diffusion barrier through the passivation layer. Therefore, we conclude that the effect of the work function modulation and electrode/nanotube contact is minor in this mechanism.

An additional mechanistic insight was obtained using Raman spectroscopy at 633 and 785 nm laser excitation before and after 18 000 ppm $SOCl_2$ injections[33] (Figure 4). Spectra from two different nanotube arrays, one exposed to 633 nm excitation and the other to 785 nm excitation, are shown (all spectra are normalized with respect to the silicon peak). A dichloromethane injection was made followed by a $SOCl_2$ injection. The former does not cause a noticeable change at 633 nm excitation but gives an overall decrease at 785 nm. Conversely, there are larger decreases in both the radial breathing modes (RBMs) and the tangential mode (G-band) after $SOCl_2$ exposure. Curiously, we note that the decrease is mainly in large diameter metallic tubes near the (13,4) feature.[34]

The radial breathing modes in this case are coupled to the c1 → v1 transition of metallic nanotubes (red indices) and the c2 → v2 transition of semiconducting nanotubes (black indices). The decrease is distinct from what is typically observed in nanotube bundle formation where a unidirectional shift in

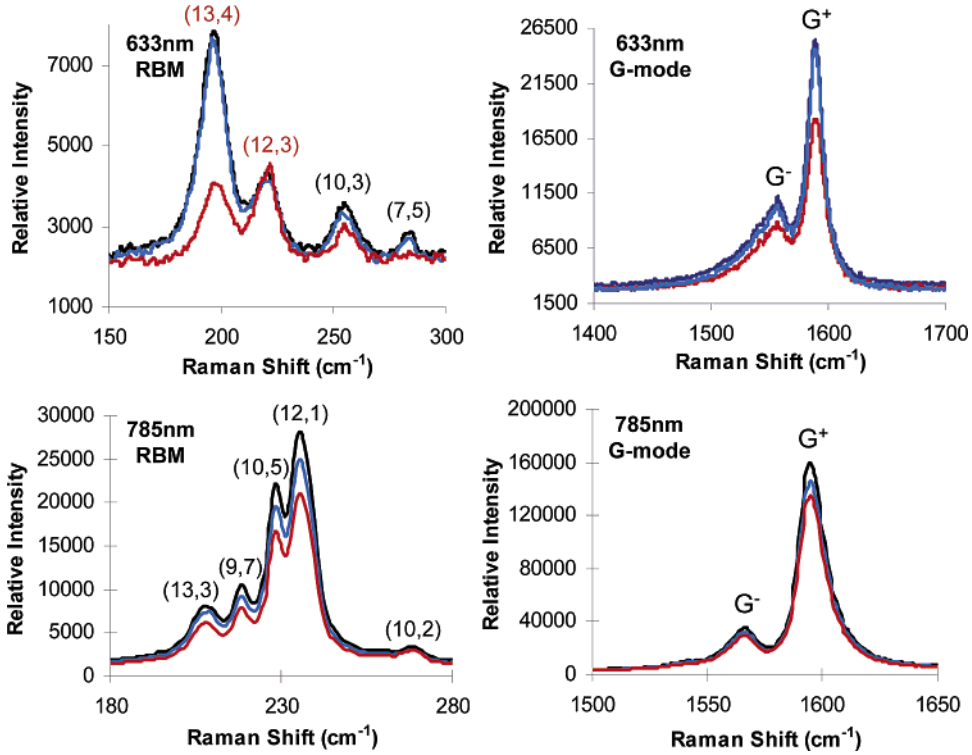

Figure 4. Raman spectra at 633 and 785 nm excitation wavelengths taken in the following order: initial (black), dichloromethane (blue), and $SOCl_2$ (red). Overall decay in both RBMs and the G-mode is observed. Among the RBMs for metallic (red indices) and semiconducting (black indices) nanotubes, the decrease in the (13,4) RBM is the most prominent suggesting the preferential electron transfer from large diameter metallic nanotubes to $SOCl_2$ molecules. The larger decrease in G^- at 633 nm rather than at 785 nm further supports this mechanism.

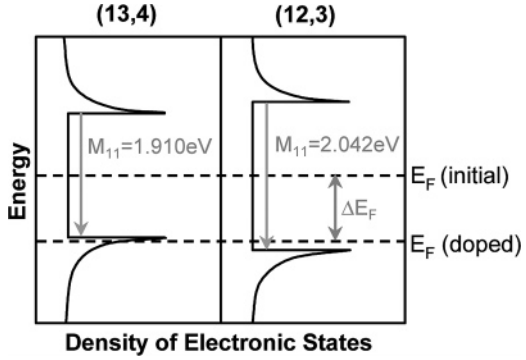

Figure 5. Proposed mechanism of selective decay in Raman and increase in current upon chemical doping. A constant Fermi level shift (ΔE_F) by electron-withdrawing $SOCl_2$ doping lowers the Fermi level below the first vHs for the (13,4), while the E_F of the (12,3) remains above. The high density of states at E_F with a depletion of electrons in the vHs of the (13,4) explains both the Raman data and electrical measurement result.

resonant energy results in either an increase or decrease for these modes for different chiralities.[35] It is plausible that there is an active flow of electrons from the SWNT array to the strongly oxidizing $SOCl_2$ molecules. A selective diminution in RBM is also observed in the covalent functionalization of metallic nanotubes.[36] There is no evidence of covalent attachment in this work as observed in the negligible D-band increase in Raman spectra (data not shown). Statistically negligible amounts of Cl and S were identified by X-ray photoelectron spectroscopy (XPS), so any residual $SOCl_2$ remaining after exposure is below the detection limit of this technique (~0.01%).

Free electrons in metallic nanotubes enable an easy electron transfer from the nanotube to $SOCl_2$. The decrease in RBMs of semiconducting nanotubes at both wavelengths is not as prominent as the decrease in the (13,4) metallic peak. This selective decay in metallic peaks is observed in the tangential mode region as well. The G^- mode at 633 nm excitation represents a characteristic feature of metallic nanotubes that can be fit using a Breit−Wigner−Fano (BWF) line shape.[37] The decrease in G^- at 633 nm with only a minor corresponding change in the G^- at 785 nm also indicates this preferential charge transfer from metallic nanotubes.

We propose that the preferential decay in the (13,4) RBM while the (12,3) peak remains constant is caused by the difference in M_{11} transition energy between the (13,4) and (12,3) nanotubes (Figure 5). We neglect the change in nanotube density of states (DOS) by $SOCl_2$ and assume there is a constant Fermi level decrease for all metallic nanotubes.[38] As the Fermi level of carbon nanotubes is lowered by $SOCl_2$ molecular adsorption, it shifts below the van Hove singularity (vHs) at the valence edge for the (13,4) and larger diameter nanotubes first, whereas the value for the (12,3) tube is still above its vHs. The estimated Fermi level after 18 000 ppm $SOCl_2$ exposure with respect to the initial level is roughly −0.988 eV in this case. At a small applied voltage (1 mV) and at low temperature, the current through the nanotube is proportional to the transmission coefficient, thus proportional to the DOS.[38−40] The increase in the occupied DOS at the Fermi level after $SOCl_2$ exposure for large diameter metallic nanotubes is the main cause of the current increase.

This Fermi level decrease helps in overcoming the tunnel barriers as well, resulting in signal increase. Nanotube/Au contacts at both electrodes were modeled as tunnel barriers with thickness a and height V_o (Figure 6a). In this asymmetric double

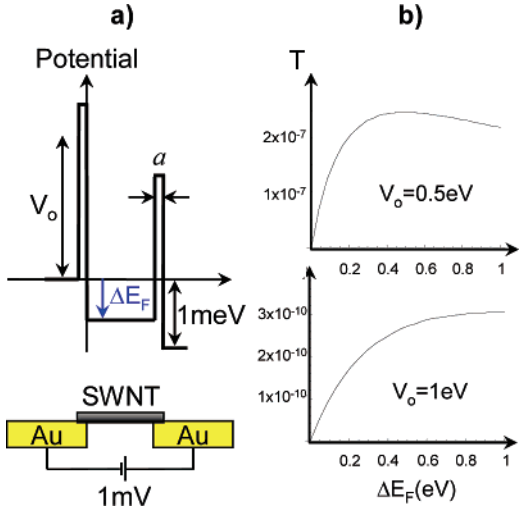

Figure 6. Electron transfer through an asymmetric double barrier. (a) Nanotube/Au contact is modeled as a tunnel barrier with height V_o and thickness a. Thionyl chloride adsorption causes Fermi level decrease (ΔE_F). (b) Transmission coefficient at two barrier heights. Fermi level decrease is shown to increase the electron transmission and thus the current.

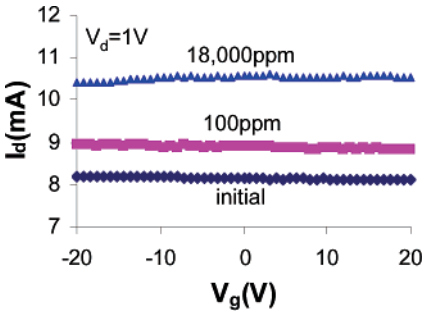

Figure 7. Channel current vs gate bias measured at different $SOCl_2$ concentrations. Small on/off ratio (~1) and vertical shift confirm that the charge transfer between SWNT and $SOCl_2$ occurs mainly through a metallic pathway.

barrier system,[41] the transmission coefficient (T) can be written as

$$T = \frac{T_L T_R}{\{1 - \sqrt{(1-T_L)(1-T_R)}\}^2 + 4\sqrt{(1-T_L)(1-T_R)}\cos^2\Phi}$$

where T_L and T_R are the transmission coefficients of the left and right barriers. Φ represents the sum of the various phase factors. T is a function of Φ and the Fermi level decrease (ΔE_F) in a SWNT due to $SOCl_2$ adsorption. Using this model, we were able to predict the enhancement of the electron transmission and, thus, the positive response to $SOCl_2$ as $SOCl_2$ lowers the SWNT Fermi level. The transmission coefficient vs ΔE_F at two barrier heights (0.5 eV and 1 eV) is shown in Figure 6b.[42] Negative responses to electron-donating DMMP could be also predicted when the sign of ΔE_F is reversed.

Raman spectroscopy probes all nanotubes excited by the excitation laser even if they do not cross the electrode gap. A semiconducting SWNT actually contributing to the conductance change can be studied by looking at the dependence on a back-gate potential. Figure 7 is a typical change in the drain current modulated by gate bias at 100 and 18 000 ppm $SOCl_2$ with a drain voltage of 1 V. Note that the gate voltage does not modulate the drain current (on/off ~ 1) meaning that semicon-

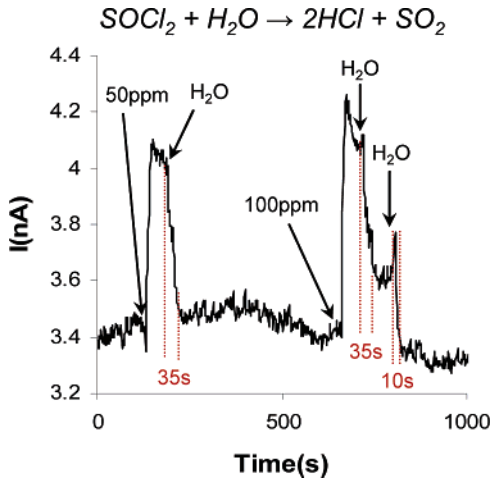

Figure 8. Rapid regeneration of the nanotube surface from irreversibly binding $SOCl_2$ molecules. Water reactive $SOCl_2$ can be hydrolyzed and desorbed from the nanotube surface by injecting water vapor on the array. The regeneration times are shown in red.

ducting nanotubes are not contributing to the signal as described by percolation theory[43,44] in a high-density nanotube network. Only a vertical shift in drain current is observed upon $SOCl_2$ injections. This is in marked contrast with the horizontal shift of a FET transfer characteristic upon analyte adsorption.[7,8,11] The small on/off ratio and vertical shift of I_d vs V_g confirm that the signal transduction occurs primarily through metallic pathways. The minor effect of the electrode/nanotube contact, shown in Figure 3, further supports this mechanism. The electrical signal transduction in conjunction with a unique selective decay in optical spectra might have implications for sensors. Currently, its performance as a $SOCl_2$ vapor sensor is limited due to the nature of the metallic SWNT. The detection limit of our $SOCl_2$ sensor array estimated over three times the noise level (10 s pulse of 3 mL of $SOCl_2$) is 3.9 ppm in average and 700 ppb at the lowest.[45]

The irreversible binding of analyte molecules is a primary hurdle for most SWNT gas sensors that have appeared in the literature to date.[1,12,13,15,46] We note that, for the system explored here, there is a facile method of regeneration by hydrolyzing reactive molecules adsorbed on the nanotube surface (Figure 8). In the case of $SOCl_2$, the decomposition by reaction with water is as follows

$$SOCl_2 + H_2O \rightarrow 2HCl + SO_2$$

The signal increase after 50 ppm $SOCl_2$ exposure is restored rapidly when a pulse of saturated water vapor at room temperature was passed over the SWNT array. A higher current increase at 100 ppm $SOCl_2$ requires two successive water injections to obtain complete restoration. For most devices, 3 mL of saturated water vapor was enough to regenerate the surface. Once the signal recovers its original value, an additional water injection causes no additional signal decrease. Hence, the response is not simply a negative response to water. We note that this method is the fastest way of regenerating a SWNT surface reported to date. Moreover, it applies to molecules capable of rapid hydrolysis which includes organophosphate chemical weapons. Low-temperature destruction of chemical agents including hydrolysis of mustard agent and nerve agent, which has been already demonstrated, supports our argument.[47] The focus on simulants of these species, such as DMMP, has obscured this chemical fact in the literature. Future studies will verify the efficacy of this method of regeneration.

Conclusion

We demonstrate and characterize, for the first time, charge transfer between SWNT and chemical vapor through predominantly metallic SWNT using dielectrophoretically deposited arrays. A selective decay of features in the Raman spectra suggests that an electrical response to $SOCl_2$ occurs mainly through large diameter metallic nanotubes. Vertical shifts of drain current upon gate modulation further supports this mechanism. This metallic SWNT array might have some applications in a sensing area although its sensitivity is limited. Hydrolysis of the adsorbed $SOCl_2$ is used to regenerate the nanotube surface. Additionally, 71 SWNT devices were tested at identical analyte concentrations, and the number of nanotubes is shown to be proportional to the conductance change on analyte binding. The normalized conductance change is shown to be constant at a fixed analyte concentration. A shift of intercept values can be used for sensor optimization. The model yields two important parameters for the class of SWNT arrays and analyte studied using this method: a maximum signal change at saturation and the rate constant of analyte adsorption.

Acknowledgment. The authors thank J. A. Rogers for providing a lithographic photomask. This work was supported by DARPA/MTO. Funding from the Dupont Young Investigator Award (2005), NSF-NIRT CCF 05-06660 funding, and a generous gift from Intel are also appreciated.

Supporting Information Available: Figure S1 shows responses to dichloromethane and thionyl chloride giving a stepwise signal increase upon exposure to thionyl chloride. Figure S2 shows responses at lower concentrations (10 ppm, 50 ppm) used to calculate k and $(\Delta G/G_o)_{max}$ in Table 1. This material is available free of charge via the Internet at http://pubs.acs.org.

References and Notes

(1) Qi, P.; Vermesh, O.; Grecu, M.; Javey, A.; Wang, O.; Dai, H. J.; Peng, S.; Cho, K. J. *Nano Lett.* **2003**, *3*, 347.

(2) Barone, P. W.; Baik, S.; Heller, D. A.; Strano, M. S. *Nat. Mater.* **2005**, *4*, 86.

(3) Peng, S.; Cho, K. J. *Nano Lett.* **2003**, *3*, 513.

(4) Peng, S.; Cho, K. J.; Qi, P. F.; Dai, H. J. *Chem. Phys. Lett.* **2004**, *387*, 271.

(5) Collins, P. G.; Bradley, K.; Ishigami, M.; Zettl, A. *Science* **2000**, *287*, 1801.

(6) Chopra, S.; McGuire, K.; Gothard, N.; Rao, A. M.; Pham, A. *Appl. Phys. Lett.* **2003**, *83*, 2280.

(7) Auvray, S.; Borghetti, J.; Goffman, M. F.; Filoramo, A.; Derycke, V.; Bourgoin, J. P.; Jost, O. *Appl. Phys. Lett.* **2004**, *84*, 5106.

(8) Auvray, S.; Derycke, V.; Goffman, M.; Filoramo, A.; Jost, O.; Bourgoin, J. P. *Nano Lett.* **2005**, *5*, 451.

(9) Star, A.; Han, T. R.; Joshi, V.; Gabriel, J. C. P.; Gruner, G. *Adv. Mater.* **2004**, *16*, 2049.

(10) Cantalini, C.; Valentini, L.; Armentano, I.; Kenny, J. M.; Lozzi, L.; Santucci, S. *J. Eur. Ceram. Soc.* **2004**, *24*, 1405.

(11) Kong, J.; Franklin, N. R.; Zhou, C. W.; Chapline, M. G.; Peng, S.; Cho, K. J.; Dai, H. J. *Science* **2000**, *287*, 622.

(12) Novak, J. P.; Snow, E. S.; Houser, E. J.; Park, D.; Stepnowski, J. L.; McGill, R. A. *Appl. Phys. Lett.* **2003**, *83*, 4026.

(13) Bekyarova, E.; Davis, M.; Burch, T.; Itkis, M. E.; Zhao, B.; Sunshine, S.; Haddon, R. C. *J. Phys. Chem. B* **2004**, *108*, 19717.

(14) Snow, E. S.; Perkins, F. K.; Houser, E. J.; Badescu, S. C.; Reinecke, T. L. *Science* **2005**, *307*, 1942.

(15) Lu, Y. J.; Li, J.; Han, J.; Ng, H. T.; Binder, C.; Partridge, C.; Meyyappan, M. *Chem. Phys. Lett.* **2004**, *391*, 344.

(16) Lee, C. Y.; Strano, M. S. *Langmuir* **2005**, *21*, 5192.

(17) Peng, S.; Cho, K. J. *Nanotechnology* **2000**, *11*, 57.

(18) Saito, R.; Dresselhaus, G.; Dresselhaus, M. S. *Physical properties of carbon nanotubes*; Imperial College Press: London, 1998.

(19) Dresselhaus, M. S.; Dresselhaus, G.; Eklund, P. C. *Science of fullerenes and carbon nanotubes*; Academic Press: San Diego, CA, 1996.
(20) Bradley, K.; Gabriel, J. C. P.; Star, A.; Gruner, G. *Appl. Phys. Lett.* **2003**, *83*, 3821.
(21) Heinze, S.; Tersoff, J.; Martel, R.; Derycke, V.; Appenzeller, J.; Avouris, P. *Phys. Rev. Lett.* **2002**, *89*.
(22) Krupke, R.; Hennrich, F.; Weber, H. B.; Kappes, M. M.; von Lohneysen, H. *Nano Lett.* **2003**, *3*, 1019.
(23) Baik, S.; Usrey, M.; Rotkina, L.; Strano, M. *J. Phys. Chem. B* **2004**, *108*, 15560.
(24) O'Connell, M. J.; Bachilo, S. M.; Huffman, C. B.; Moore, V. C.; Strano, M. S.; Haroz, E. H.; Rialon, K. L.; Boul, P. J.; Noon, W. H.; Kittrell, C.; Ma, J. P.; Hauge, R. H.; Weisman, R. B.; Smalley, R. E. *Science* **2002**, *297*, 593.
(25) Zheng, M.; Jagota, A.; Strano, M. S.; Santos, A. P.; Barone, P.; Chou, S. G.; Diner, B. A.; Dresselhaus, M. S.; McLean, R. S.; Onoa, G. B.; Samsonidze, G. G.; Semke, E. D.; Usrey, M.; Walls, D. J. *Science* **2003**, *302*, 1545.
(26) The response to dichloromethane is either negative or positive in some cases, but the response is small compared with the $SOCl_2$ response.
(27) See the Supporting Information.
(28) The responses from two different gap sizes are plotted together since they fall on the same line.
(29) The r^2 values are 0.937, 0.977, and 0.992 for systems 1, 2, and 3, respectively.
(30) Masel, R. I. *Principles of adsorption and reaction on solid surfaces*; Wiley: New York, 1996.
(31) Zhang, Z. B.; Cardenas, J.; Campbell, E. E. B.; Zhang, S. L. *Appl.Phys. Lett.* **2005**, *87*.
(32) See the Supporting Information for 10 and 50 ppm data.
(33) 100 ppm $SOCl_2$ did show a slight decrease, but it was not evident enough to explain the preferential decrease in the Raman features which are discussed in this work.
(34) Strano, M. S. *J. Am. Chem. Soc.* **2003**, *125*, 16148.
(35) Heller, D. A.; Barone, P. W.; Swanson, J. P.; Mayrhofer, R. M.; Strano, M. S. *J. Phys. Chem. B* **2004**, *108*, 6905.
(36) Strano, M. S.; Dyke, C. A.; Usrey, M. L.; Barone, P. W.; Allen, M. J.; Shan, H. W.; Kittrell, C.; Hauge, R. H.; Tour, J. M.; Smalley, R. E. *Science* **2003**, *301*, 1519.
(37) Brown, S. D. M.; Jorio, A.; Corio, P.; Dresselhaus, M. S.; Dresselhaus, G.; Saito, R.; Kneipp, K. *Phys. Rev. B* **2001**, *63*, 155414.
(38) Dettlaff-Weglikowska, U.; Skakalova, V.; Graupner, R.; Jhang, S. H.; Kim, B. H.; Lee, H. J.; Ley, L.; Park, Y. W.; Berber, S.; Tomanek, D.; Roth, S. *J. Am. Chem. Soc.* **2005**, *127*, 5125.
(39) Datta, S. *Nanotechnology* **2004**, *15*, S433.
(40) Orlikowski, D.; Mehrez, H.; Taylor, J.; Guo, H.; Wang, J.; Roland, C. *Phys. Rev. B* **2001**, *6315*.
(41) Ferry, D. K.; Goodnick, S. M. *Transport in nanostructures*; Cambridge University Press: Cambridge, U.K., 1997.
(42) $a = 1$ nm, electron energy of 1 meV, and $\Phi = 2\pi/5$ are assumed in this calculation. Using other values gives a similar trend. See ref 41 for detailed calculations.
(43) Bo, X. Z.; Lee, C. Y.; Strano, M. S.; Goldfinger, M.; Nuckolls, C.; Blanchet, G. B. *Appl. Phys. Lett.* **2005**, *86*.
(44) Hu, L.; Hecht, D. S.; Gruner, G. *Nano Lett.* **2004**, *4*, 2513.
(45) These detection limits are from devices made by the deposition of HiPco SWNT suspended in SDS.
(46) Li, J.; Lu, Y. J.; Ye, Q.; Cinke, M.; Han, J.; Meyyappan, M. *Nano Lett.* **2003**, *3*, 929.
(47) Pearson, G. S.; Magee, R. S. *Pure Appl. Chem.* **2002**, *74*, 187.